Editors' Suggestion | Featured in Physics

Measurement of Capillary Forces Using Two Fibers Dynamically Withdrawn from a Liquid: Evidence for an Enhanced Cheerios Effect

Hadrien Bense,* Emmanuel Siéfert,† and Fabian Brau‡
Université libre de Bruxelles (ULB), Nonlinear Physical Chemistry Unit, CP 231, 1050 Bruxelles, Belgium

(Received 20 December 2022; accepted 12 September 2023; published 3 November 2023)

We study the capillary attraction force between two fibers dynamically withdrawn from a bath. We propose an experimental method to measure this force and show that its magnitude strongly increases with the retraction speed by up to a factor of 10 compared to the static case. We show that this remarkable increase stems from the shape of the dynamical meniscus between the two fibers. We first study the dynamical meniscus around one fiber and obtain experimental and numerical scaling of its size increase with the capillary number, which is not captured by the classical Landau-Levich-Derjaguin theory. We then show that the shape of the deformed air-liquid interface around two fibers can be inferred from the linear superposition of the interface around a single fiber. These results yield an analytical expression for the capillary force which compares well with the experimental data. Our study reveals the critical role of the retraction speed to create stronger capillary interactions, with potential applications in industry or biology.

DOI: 10.1103/PhysRevLett.131.184003

Dip coating is a technique consisting in drawing an object out of a liquid bath to apply a coating layer [1–3]. It is used in industry to functionalize objects with, e.g., antireflective [4], biocompatible [5], hydrophobic [6], or electrothermal [7] coatings. This process is also used by some animals, such as bees, bats, or birds, to feed by dipping their brushlike tongue in nectar [8–10]. When several objects are dipped simultaneously in a liquid, each of them deforms the interface, which induces a force acting on its neighbors [11]. This long-range capillary interaction, known as the "Cheerios effect" [12–19], is mediated by the shape of the meniscus surrounding the objects. Beyond its fundamental interest, the Cheerios effect has been recently harnessed in the context of particle self-assembly [17,18,20]. However, the effect of dynamics on the Cheerios effect, when, e.g., flexible dip-coated structures are swiftly removed from a bath, remains poorly investigated.

Dip coating is usually studied with the Landau-Levich-Derjaguin (LLD) theory which predicts that, for a thin fiber removed at sufficiently small speed from a bath of Newtonian liquid, the thickness of the film deposited on the fiber is given by [21–24]

$$t = 1.34 R \mathrm{Ca}^{2/3}, \tag{1}$$

where R is the fiber radius, $\mathrm{Ca} = \mu V/\gamma$ the capillary number, μ the viscosity, γ the surface tension of the liquid, and V the withdrawal speed. This relation has been obtained in a regime where the Reynolds number $\mathrm{Re} = \rho V R/\mu$ and the Bond number $\mathrm{Bo} = R^2/\ell_c^2$ are small ($\ell_c = \sqrt{\gamma/\rho_\ell g}$ is the capillary length, ρ_ℓ the liquid density, and g the gravitational acceleration). This relation was proved successful for Ca up to roughly 0.03 [see Supplemental Material [25], Fig. S2(b)] and has been extended to larger Ca, Bo, and Re [24,26–34] and to different liquids such as partially wetting [35], suspension [36,37], non-Newtonian [38–40], polymer [41,42], and surfactant [43–45] solutions (see also the recent review [46]). The LLD model essentially assumes that the thin lubricated film deposited on the fiber connects to the static meniscus.

In this Letter, we rationalize the capillary menisci-mediated interaction between two fibers as they are dynamically withdrawn from a liquid bath. Building on our previous work studying the coalescence of two static partially immersed fibers [11], we develop an original measurement technique, based on the deflection of elastic fibers, to experimentally access the dynamical capillary force. We show that it may be one order of magnitude larger than the static force computed in Ref. [13]. To understand this large increase of force, we analyze the dynamical meniscus around two fibers pulled out of a bath and show that it can be reconstructed from the static meniscus around a single fiber. We then draw analogy from the static case to derive an expression of the capillary interaction accounting for the large force measured.

The experiments are performed with two identical fibers of length L and radius R clamped vertically to a linear stage at a distance $2d$ and immersed in a silicone oil bath; see Fig. 1(a) and Ref. [25]. The first step of the experiment consists in determining the dry length L_s of the fibers at which the attraction force created by the static meniscus can bend the two fibers enough to trigger their coalescence. Following the procedure described in Ref. [11], the fibers

are quasistatically removed from the bath to determine L_s. The fibers are then shortened at a length $L < L_s$, such that the static capillary attraction is not strong enough to induce their coalescence. The shortened fibers are then dynamically withdrawn out of the bath at constant speed V. The deformation of the air-liquid interface increases with V, and, as a result, the distance δ between the fiber free ends decreases. For a threshold speed $V = V_c$, the two fibers coalesce [Fig. 1(a) and Movie 1 in Supplemental Material [25]]. Once V_c is found for a given L, the fibers are shortened again, and the subsequent threshold retraction speed is determined. This shortening process is repeated until the fibers are too short to coalesce at any retraction speed considered (Re $\lesssim 10^{-2}$ and Ca $\lesssim 0.5$). Shortening the fibers ensure that, when coalescence occurs, the immersed part of both fibers is sufficiently small to neglect any viscous drag acting on the structures. This iterative process yields the critical speed V_c at which two fibers of length L coalesce. Figure 1(b) shows that L decreases as V increases, demonstrating that the Cheerios effect between the two fibers is enhanced by their dynamical withdrawal.

As shown in Ref. [11] for the quasistatic case, coalescence occurs when the lateral force due to capillarity, $F_s = \gamma\pi R^2/\delta$, equals the elastic force, $F_{\rm el} = 3B\delta/L^3$, required to bend the fibers over a distance $\delta = d/2$. As seen in Fig. 1(c), the relation $F_s(d/2) = F_{\rm el}(d/2)$ is recovered at Ca $= 0$. This suggests to plot Bd/L^3 as a function of the capillary number Ca to estimate the dynamic capillary force F. Figure 1(d) shows that F decreases as d/R increases, like in the static case, but increases up to one order of magnitude when Ca increases at fixed d/R. Hence, dynamic withdrawal of immersed objects increases notably their capillary interaction compared to the static case.

The interaction between the fibers is mediated by the meniscus created around them [11,13,19]. To get some insights into the deformation of the air-liquid interface as the fibers are withdrawn from the bath, the dynamical meniscus around a single fiber is first analyzed. Figures 2(a) and 2(b) show that it grows significantly with the withdrawal speed. However, Fig. 2(c) shows that rescaling the menisci height by $1 + \zeta(\mathrm{Ca})$ leads to a

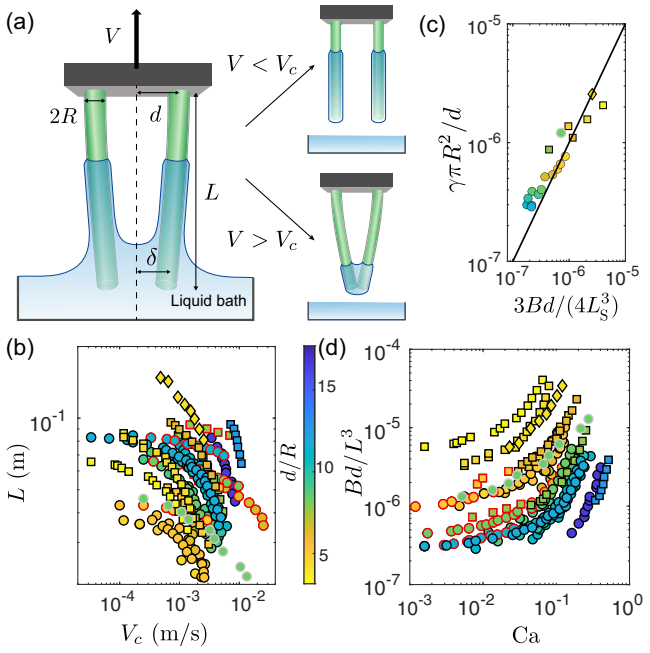

FIG. 1. (a) Experimental setup. Two parallel glass fibers separated by a distance $2d$ and clamped at one end are removed from a fluid bath at a speed V ($E = 64 \pm 1$ GPa). Above a critical velocity V_c, the fibers coalesce. (b) Length L of the fibers as a function of V_c. Squares, $R = 100$ μm; circles, $R = 50$ μm; diamonds, $R = 160$ μm. Face color represents d/R given by the color bar; edge color corresponds to the fluid properties; black, silicon oil V1000 ($\mu = 0.96$ Pa s); red, silicon oil V100 ($\mu = 0.096$ Pa s); gray, glycerol ($\mu = 1.3$ Pa s). $\gamma = 0.021$ N m^{-1} for silicon and 0.063 N m^{-1} for glycerol. (c) At $V = 0$ m/s, the scaling for $L = L_s$ obtained in Ref. [11] is recovered (solid curve). (d) Estimation of the dynamic capillary force Bd/L^3 as a function of Ca.

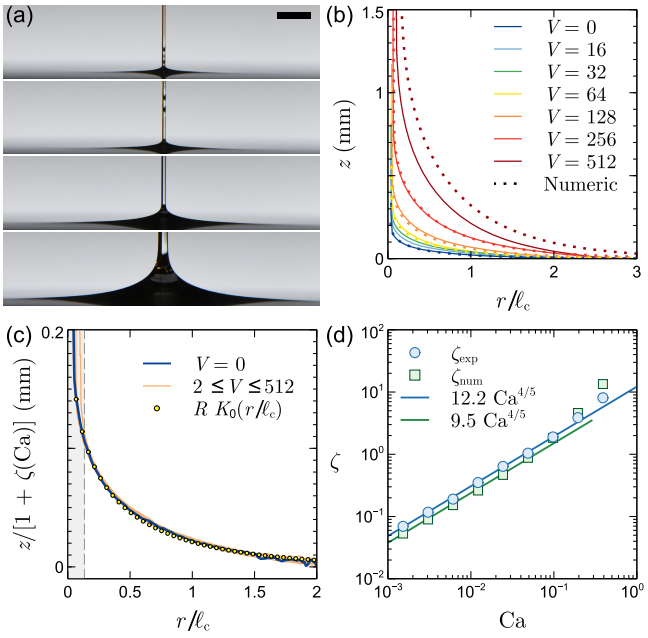

FIG. 2. (a) Snapshots of a glass fiber ($R = 50$ μm) withdrawn from silicon oil ($\mu = 0.96$ Pa s) at various retraction speeds ($V = 0$, 16, 128, 512 mm/ min). Scale bar: 1 mm. (b) Meniscus shape as a function of the rescaled radial distance r/ℓ_c at various V (mm/min). The agreement with the theoretical model proposed in Ref. [24] is good up to $V = 256$ mm/ min (Ca $\simeq 0.2$). (c) Collapse of the dynamical meniscus profiles onto the static meniscus shape when their height are properly rescaled by $1 + \zeta$. $V = 2^n$ mm/ min with $1 \le n \le 9$. The gray shaded area indicates the region where the collapse is not satisfactory for the largest retraction speed. (d) Evolution of the scaling factor ζ as a function of Ca. $\zeta_{\rm exp}$ and $\zeta_{\rm num}$ correspond to the experimental and numerical profiles, respectively [25].

collapse of the profiles onto the static meniscus which, in turn, is well approximated by the modified Bessel function of the second kind of zeroth-order K_0 [12,19,47,48]. The collapse is satisfactory provided $r \gtrsim 4R$ for the investigated retraction speeds. A similar collapse is obtained for the theoretical profiles computed with the model proposed in Ref. [24] (see Supplemental Material [25]). The quantity ζ scales as $\mathrm{Ca}^{4/5}$ for both the experimental and numerical profiles yet with a slightly different prefactor [Fig. 2(d)]. This increase of the vertical elevation of the meniscus is related to the film thickening [25]. Indeed, the meniscus height, far enough from the fiber, is proportional to the fiber radius, i.e., $z \simeq RK_0(r/\ell_c)$, which is effectively increased by the deposited film. For the values of Ca considered here, t increases faster than $\mathrm{Ca}^{2/3}$ [25], leading to a larger exponent for ζ, i.e., $4/5$.

To analyze the dynamical meniscus created by two withdrawn fibers, two identical clamped fibers are pulled out of a liquid bath. They are sufficiently short to not significantly deflect during their withdrawal. The shape of the air-liquid interface is measured in a stationary regime for various R, d, γ, and μ [Figs. 3(a) and 3(b)]. For the range of d considered here and $\mathrm{Ca} \lesssim 0.2$ [25], the profile of the dynamical meniscus around two fibers, $z_{d,2}$, is given in good approximation by $z_{d,2}(x,y) = z_{d,1}(x-d,y) + z_{d,1}(x+d,y)$, where $z_{d,1}$ is the profile of the dynamical meniscus around a single fiber centered at $x = y = 0$ [see Fig. 3(c) and Ref. [25]]. Since Fig. 2 shows that $z_{d,1} = (1+\zeta)z_{s,1}$, where $z_{s,1}$ is the profile of the static meniscus around a single fiber, the height of the liquid bridge $h = z_{2,d}(0,0)$ can, thus, be expressed as

$$h = h_s(1+\zeta), \qquad \zeta \simeq 12.2\mathrm{Ca}^{4/5}, \tag{2a}$$

$$h_s = 2RK_0(d/\ell_c) \simeq 2R\ln[2\ell_c/(\gamma_e d)], \tag{2b}$$

where h_s is the height of the liquid bridge between two fibers at $\mathrm{Ca} = 0$ [Fig. 3(a)] and where the second expression in Eq. (2b) is obtained from the expansion of K_0 for $d \ll \ell_c$ with $\gamma_e \simeq 1.781$ the exponential of the Euler-Mascheroni constant. Figure 3(d) shows that the relative variation of the measured bridge height, $\Delta h/h_s$, varies in good approximation as ζ, as expected from Eq. (2a). Note that the data in Fig. 3(d) have been rescaled by powers of R/d (see Supplemental Material [25] for the data without this rescaling). Indeed, for a given system, there is a critical retraction speed beyond which a liquid column is entrained between both fibers and the dynamical meniscus is no longer stationary [see vertical dashed lines in Fig. 3(d) and Movie 2 in Supplemental Material [25]]. This happens when the coating film thickness on each fiber $t \sim R\mathrm{Ca}^{2/3}$ reaches a fraction of the distance d, i.e., when $(R/d)^{3/2}\mathrm{Ca} \simeq 0.02$. Right below this threshold, for $0.01 \lesssim \mathrm{Ca}(R/d)^{3/2} \lesssim 0.02$, the dynamical meniscus is still stationary but may no longer be obtained by linear

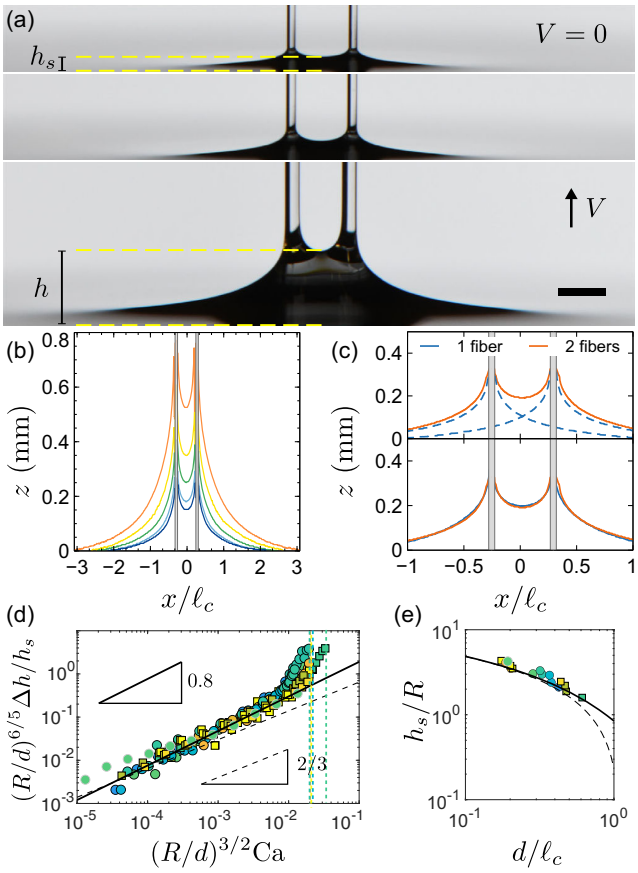

FIG. 3. (a) Snapshots of two glass fibers ($R = 100$ μm) withdrawn from silicon oil ($\mu = 0.96$ Pa s) at $V = 0$, 32, 256 mm/min. Scale bar: 1 mm. (b) Meniscus profiles as V increases (0, 8, 32, 64, 128 mm/min). (c) Comparison between the dynamical meniscus around two fibers ($R = 50$ μm) separated by a distance $2d = 0.88$ mm and withdrawn at $V = 16$ mm/min ($\mathrm{Ca} = 0.012$, orange curve) and the meniscus (solid blue curve) obtained by summing the dynamical meniscus around a single fiber withdrawn at the same speed (dashed blue curve). (d) Evolution of $\Delta h/h_s$ as a function of Ca. All data collapse on the same power law as the one obtained in Fig. 2(d): $\Delta h/h_s = 12.2\mathrm{Ca}^{4/5}$. An increase of slope is observed when $d \simeq 20R\mathrm{Ca}^{2/3}$. The vertical dashed lines correspond to the threshold above which a liquid film is entrained. (e) Height of the static bridge as a function of the fibers distance. The solid curve corresponds to Eq. (2b) and the dashed curve to its logarithmic approximation valid for $d/\ell_c \ll 1$. See Fig. 1 for the symbol and color code.

superposition, because h drastically increases, inducing a noticeable change of slope in Fig. 3(d) [25]. To capture this change of slope and obtain a good collapse of the data, Ca needs to be rescaled by $(R/d)^{3/2}$ and, accordingly, $\Delta h/h_s$ by $[(R/d)^{3/2}]^{4/5} = (R/d)^{6/5}$. Note also that the measured static liquid bridge height h_s, displayed in Fig. 3(e), is well described by Eq. (2b).

We now rationalize the dynamical force acting on two fibers during their withdrawal [Fig. 1(d)]. We follow the

approach developed in Ref. [13] to compute the shape of the meniscus around two static fibers and the resulting capillary force. Note that this approach is, *a priori*, valid only for small meniscus slopes ($\theta_Y \simeq \pi/2$). However, Eq. (2b) coincides with the expression of h_s obtained with this approach, and Fig. 3(e) shows that it gives a good description of the data even for $\theta_Y = 0$. In addition, we have shown that the capillary force obtained in Ref. [13] gives a good description of the coalescence of two static fibers when $\theta_Y = 0$ [11]. In the following, we thus use $\theta_Y = 0$. In this case, the difference of surface energy, U_S, between a configuration where two vertical fibers of radius R are at an infinite distance and the one where they are at a distance $2d$ [Fig. 1(a)] reads as

$$U_S = -2\pi\gamma R(H_d - H_\infty), \tag{3}$$

where H_d and H_∞ are the mean elevations of the (static) meniscus contact line on each fiber when they are, respectively, at a distance $2d$ or at infinity. When $d \gg R$, this difference is given by [11,13]

$$H_d - H_\infty = R\ln[\ell_c/(2d\gamma_e)] = h_s/2 - 2R\ln 2, \tag{4}$$

where we used the logarithmic approximation of h_s; see Eq. (2b). The static capillary force is given by $2F_s = -\partial U_S/\partial d$:

$$F_s(d) = \frac{\pi}{2}\gamma R\frac{\partial h_s}{\partial d} = -\frac{\pi\gamma R^2}{d}. \tag{5}$$

In both the static and the dynamical cases, the capillary force is mediated by the meniscus; therefore, we assume that the interaction energy (3) and the method to derive the capillary force still apply with the static meniscus replaced by the dynamical one. We, thus, obtain

$$F(d) = \frac{\pi}{2}\gamma R\frac{\partial h}{\partial d} = (1+\zeta)F_s(d), \qquad \zeta \simeq 12.2\mathrm{Ca}^{4/5}. \tag{6}$$

Figure 4 shows that the relative variation of the dynamical capillary force, $\Delta F/F_s$, computed from the raw data reported in Fig. 1(d), varies in good approximation as ζ in agreement with Eq. (6). Note that the data in Fig. 4 have been again rescaled by powers of R/d to capture the observed change of slope. The physical mechanism behind this change of slope is similar as in Fig. 3(d), but, since the fibers bend toward each other by typically half their initial distance before coalescing as they are withdrawn [11,25], the change of slope is expected to occur at $(R/d)^{3/2}\mathrm{Ca} \simeq 0.01/2^{3/2} \simeq 4\times10^{-3}$, which agrees with the onset of slope change in Fig. 4.

Equation (6) shows that dynamical interaction between two fibers withdrawn from a liquid bath at a finite speed is equivalent to the static interaction with an effective surface tension increasing with the capillary number, i.e.,

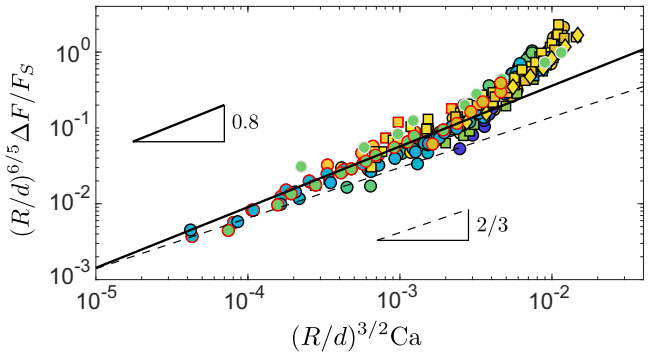

FIG. 4. Evolution of $\Delta F/F_s$ as a function of Ca. All data collapse on the same power law as the one obtained in Fig. 2(d): $\Delta F/F_s = 12.2\mathrm{Ca}^{4/5}$. An increase of slope is observed when $d \simeq 50R\mathrm{Ca}^{2/3}$. See Fig. 1 for the symbol and color code.

$\gamma_{\mathrm{eff}} = \gamma(1+\zeta)$. It appears, thus, that the potential hydrodynamic effects in the bath are negligible, as in the case of fiber sedimentation [49]. Consequently, all the analysis performed for the static case can be easily reproduced [11]. For example, neglecting tension in the fibers and assuming $d \gg R$ to keep the algebra simple here, the critical fiber length beyond which coalescence occurs during the withdrawal at finite speed is given by

$$L^3 = \frac{L_s^3}{1+\zeta} = \frac{3Bd^2}{4\pi\gamma R^2}(1+\zeta)^{-1}, \tag{7}$$

where L_s is the corresponding length in the static case. Hence, L is reduced by 25% compared to L_s at $\mathrm{Ca} \simeq 0.065$ and by 50% at $\mathrm{Ca} \simeq 0.5$.

In the case of partially wetting liquids ($\theta_Y > 0$), the increase in force is even more spectacular. For example, in the extreme case where $\theta_Y = \pi/2$, the interaction force vanishes in the static case, as the air-liquid interface is not deformed by the fibers. At finite retraction speed, however, the viscous entrainment along the fibers leads to the deformation of the interface and to a new dynamic contact angle, leading to a finite capillary force [50,51].

In summary, we have studied experimentally and theoretically the withdrawal of two fibers out of a liquid bath. To account for the steep increase of the capillary attractive force, we first showed that the shape of the dynamical meniscus around one fiber can be obtained by scaling the shape of the static meniscus by a factor depending on Ca. We then experimentally demonstrated that the air-liquid interface between two withdrawn fibers is in good approximation described by the linear superposition of the interface around one fiber. With these ingredients, we derived analytical expressions for the evolution of the attraction force with Ca and the critical fiber length beyond which two fibers coalesce at a given Ca. A natural prolongation of this work is to consider an array of fibers to study potential collective effects on the onset of coalescence and on the

shape of the coalesced states, i.e., single or multiple coalesced bundle of fibers. Indeed, recent experiments show that retraction speed strongly influence the coalesced shape [52,53]. The influence of coalescence on the amount of fluid stored in an array of fibers is also of interest to optimize fluid capture with potential applications to rationalize the nectar feeding by some passerine birds characterized by a brushlike tongue [10,54]. Finally, we note that the retraction speed appears to be an interesting parameter to fine-tune the capillary interaction force between slender structures. It may open new possibilities for the capillary self-assembly of particles and fibers at fluid interfaces [20,55].

The authors acknowledge support by the Fund for Scientific Research (F.R.S.-FNRS) under Research Grant No. J.0017.21 (CDR "FASTER") and by the Federation Wallonia-Brussels (FWB) (Concerted Research Actions "Capture"). This project has received funding from the European Union's Horizon 2020 research and innovation programme under the Marie Sklodowska-Curie Grant Agreements No. 101027862 and No. 101102728. This project also has received the support of ULB incentives measures, available thanks to the FWB, to foster participation to European Union projects.

H. B. and E. S. contributed equally to this work.

*hadrien.bense@ulb.be
†emmanuel.siefert@ulb.be
‡fabian.brau@ulb.be

[1] K. J. Ruschak, Annu. Rev. Fluid Mech. **17**, 65 (1985).
[2] S. J. Weinstein and K. J. Ruschak, Annu. Rev. Fluid Mech. **36**, 29 (2004).
[3] P. M. Schweizer and S. F. Kistler, *Liquid Film Coating: Scientific Principles and their Technological Implications* (Springer Science & Business Media, New York, 2012).
[4] A. Jonsson, A. Roos, and E. K. Jonson, Sol. Energy Mater Sol. Cells **94**, 992 (2010).
[5] E. Mohseni, E. Zalnezhad, and A. R. Bushroa, Int. J. Adhes. Adhes. **48**, 238 (2014).
[6] C. Kapridaki and P. Maravelaki-Kalaitzaki, Progr. Org. Coating **76**, 400 (2013).
[7] D. Janas and K. K. Koziol, Nanoscale **6**, 3037 (2014).
[8] A. Lechantre, A. Draux, H.-A. B. Hua, D. Michez, P. Damman, and F. Brau, Proc. Natl. Acad. Sci. U.S.A. **118**, e2025513118 (2021).
[9] C. J. Harper, S. M. Swartz, and E. L. Brainerd, Proc. Natl. Acad. Sci. U.S.A. **110**, 8852 (2013).
[10] R. J. Mitchell and D. C. Paton, Oecologia **83**, 238 (1990).
[11] E. Siéfert, H.-A. B. Hua, and F. Brau, Extreme Mech. Lett. **55**, 101823 (2022).
[12] M. M. Nicolson, in *Mathematical Proceedings of the Cambridge Philosophical Society* (Cambridge University Press, Cambridge, England, 1949), Vol. 45, pp. 288–295.
[13] P. A. Kralchevsky, V. N. Paunov, I. B. Ivanov, and K. Nagayama, J. Colloid Interface Sci. **151**, 79 (1992).
[14] P. A. Kralchevsky and N. D. Denkov, Curr. Opin. Colloid Interface Sci. **6**, 383 (2001).
[15] D. Vella and L. Mahadevan, Am. J. Phys. **73**, 817 (2005).
[16] I. Ho, G. Pucci, and D. M. Harris, Phys. Rev. Lett. **123**, 254502 (2019).
[17] L. Botto, E. P. Lewandowski, M. Cavallaro, and K. J. Stebe, Soft Matter **8**, 9957 (2012).
[18] R. McGorty, J. Fung, D. Kaz, and V. N. Manoharan, Mater. Today **13**, 34 (2010).
[19] H. Cooray, P. Cicuta, and D. Vella, J. Condens. Matter Phys. **24**, 284104 (2012).
[20] C. Zeng, M. W. Faaborg, A. Sherif, M. J. Falk, R. Hajian, M. Xiao, K. Hartig, Y. Bar-Sinai, M. P. Brenner, and V. N. Manoharan, Nature (London) **611**, 68 (2022).
[21] B. V. Derjaguin, C. R. (Dokl.) Acad. Sci. URSS **39**, 13 (1943).
[22] B. V. Derjaguin, Prikl. Mekh. Tekh. Phys. **3**, 71 (1963).
[23] D. Quéré, Annu. Rev. Fluid Mech. **31**, 347 (1999).
[24] Z. Zhang, A. Salamatin, F. Peng, and K. G. Kornev, J. Colloid Interface Sci. **607**, 502 (2022).
[25] See Supplemental Material at http://link.aps.org/supplemental/10.1103/PhysRevLett.131.184003 for movies and details about the experimental methods and the theoretical model.
[26] J. A. Tallmadge, R. A. Labine, and B. H. Wood, Ind. Eng. Chem. Fundam. **4**, 400 (1965).
[27] D. A. White and J. A. Tallmadge, Chem. Eng. Sci. **20**, 33 (1965).
[28] D. A. White and J. A. Tallmadge, AIChE J. **12**, 333 (1966).
[29] R. S. Burkina and V. I. Vilyunov, Fluid Dyn. **15**, 835 (1980).
[30] S. D. R. Wilson, J. Eng. Math. **16**, 209 (1982).
[31] A. Koulago, V. Shkadov, D. Quéré, and A. de Ryck, Phys. Fluids **7**, 1221 (1995).
[32] A. de Ryck and D. Quéré, J. Fluid Mech. **311**, 219 (1996).
[33] A. de Ryck and D. Quéré, J. Colloid Interface Sci. **203**, 278 (1998).
[34] E. S. Benilov and V. S. Zubkov, J. Fluid Mech. **617**, 283 (2008).
[35] J. H. Snoeijer, J. Ziegler, B. Andreotti, M. Fermigier, and J. Eggers, Phys. Rev. Lett. **100**, 244502 (2008).
[36] A. Gans, E. Dressaire, B. Colnet, G. Saingier, M. Z. Bazant, and A. Sauret, Soft Matter **15**, 252 (2019).
[37] S. Palma and H. Lhuissier, J. Fluid Mech. **869** (2019).
[38] P. Tanguy, M. Fortin, and L. Choplin, Int. J. Numer. Methods Fluids **4**, 459 (1984).
[39] K. Afanasiev, A. Münch, and B. Wagner, Phys. Rev. E **76**, 036307 (2007).
[40] J. Ashmore, A. Q. Shen, H. P. Kavehpour, H. A. Stone, and G. H. McKinley, J. Eng. Math. **60**, 17 (2008).
[41] A. de Ryck and D. Quéré, Langmuir **14**, 1911 (1998).
[42] Z. Zhang, F. Peng, and K. G. Kornev, Micromachines **13**, 982 (2022).
[43] D. Quéré, A. de Ryck, and O. Ou Ramdane, Europhys. Lett. **37**, 305 (1997).
[44] A. Q. Shen, B. Gleason, G. H. McKinley, and H. A. Stone, Phys. Fluids **14**, 4055 (2002).
[45] H. C. Mayer and R. Krechetnikov, Phys. Fluids **24**, 052103 (2012).
[46] E. Rio and F. Boulogne, Adv. Colloid Interface Sci. **247**, 100 (2017).
[47] *NIST Handbook of Mathematical Functions*, edited by F. W. J. Olver, D. W. Lozier, R. F. Boisvert, and

C. W. Clark (Cambridge University Press, Cambridge, England, 2010).
[48] L. L. Lo, J. Fluid Mech. **132**, 65 (1983).
[49] E. Guazzelli and J. Hinch, Annu. Rev. Fluid Mech. **43**, 97 (2011).
[50] T. S. Chan, J. H. Snoeijer, and J. Eggers, Phys. Fluids **24**, 072104 (2012).
[51] T. Shing Chan, T. Gueudré, and J. H. Snoeijer, Phys. Fluids **23**, 112103 (2011).
[52] L. Kovanko and S. Tawfick, Langmuir **35**, 13421 (2019).
[53] J. Ha, Y. S. Kim, K. Jiang, R. Siu, and S. Tawfick, Phys. Rev. Lett. **125**, 254503 (2020).
[54] Y.-M. Chang, H.-Y. Lin, K. A. Hatch, C.-T. Yao, and H.-J. Shiu, Wilson J. Ornithol. **125**, 204 (2013).
[55] B. Pokroy, S. H. Kang, L. Mahadevan, and J. Aizenberg, Science **323**, 237 (2009).